Acoustic Source Localization with a VTOL sUAV Deployable Module

by

Kory Olney

A thesis submitted in partial fulfillment
of the requirements for the degree of
Master of Science in Mechanical Engineering
Department of Mechanical Engineering
College of Engineering
University of South Florida

Major Professor: Robert Bishop, Ph.D.
Jonathan Gaines, Ph.D.
Michael Guinn, M.S.B.E.

Date of Approval:
October 31, 2018

Keywords: FPGA, DSP, DOA, Drone,
LabVIEW, Active Shooter

DEDICATION

The efforts put forth in the completion of this research are dedicated to the USA's military members and law enforcement officers that bravely respond to the sound of hostile gunfire. The sacrifices of these selfless men and women often go either unknown or under appreciated by those they serve and protect. Without individuals willing to forgo the personal comforts of modern life, our communities would not be able to enjoy the safety that we often take for granted.

ACKNOWLEDGMENTS

This research was partially supported by USSOCOM, through a partnership intermediary agreement with DEFENSEWERX. The public facing intermediary known as SOFWERX supervised this effort by providing financial support, equipment, and lab space to build and evaluate the system. The guidance from an assortment of engineers provided me support throughout the development of this project.

Thank you to my supervisor Dr. Robert H. Bishop for his guidance and for finding funding for the assistantship. Thank you to my other committee member Dr. Jonathan Gaines, and Michael Guinn for providing support and guidance throughout the life of this research.

I would like to thank Pasco County Sherriff's Office for allowing me to acquire data at their outdoor shooting facility. With their cooperation I was able to record the acoustic signatures of a variety of calibers that can be used as a reference when providing gunshot detection and characterization. This data will be used for many years to come.

TABLE OF CONTENTS

LIST OF TABLES

LIST OF FIGURES

ABSTRACT

A real time acoustic direction-finding module has been developed to estimate the elevation and azimuth of an impulsive event while functioning onboard a small unmanned aircraft vehicle. The generalized cross-correlation with phase transform method was used to estimate time differences of arrival in an eight channel microphone array. A linear least squares approach was used to calculate an estimate for the direction of arrival. In order to accomplish this task, a vertical takeoff and landing small unmanned aircraft system was assembled to host the direction-finding module. The module itself is made up of an eight-channel synchronous analog-to-digital converter connected to eight lightweight micro electro-mechanical microphones with pre-amplifiers. The data is processed on an embedded system with a field programmable gate array chip and a central processing unit. Noise canceling techniques were employed to address the noise propagating from the propellers under operation. The results from this research show that it is possible to perform direction-finding estimation while aboard an operating small unmanned aircraft vehicle with initial tests showing maximum errors of $\pm\ 7^{\circ}$.

CHAPTER 1: INTRODUCTION

1.1 Motivation

Developments in small unmanned aircraft systems (sUAS) within the past decade have created an environment of tremendous potential that is currently affecting many industries. While the complexity of these systems continues to increase, high-volume production is leading to a decrease in cost as more private consumers gain access to these systems. The technology has matured to the point that it will undoubtedly play an integral part of future developments across many industries.

Modern living is increasingly being redefined by new technologies as the rapid pace of innovation in the private sector continues to produce low cost systems that contest traditional technologies. The rise in availability of sUAS presents new threats as well as new capabilities. One of the key benefits that sUAS provide is the rapid deployment of various sensors to a specific location that can process data to increase situational awareness on the ground in real-time.

Sensors are becoming smaller and less expensive while providing more computational power. The sUAS industry has benefited from many open source contributions in software and hardware originating from the hobbyist radio control (RC) market.

1.2 Objectives

This thesis has three main objectives,

1. Construct a low-cost prototype sUAS with a payload capacity of at least 4 lb,

2. Construct a microphone sensor array that addresses constraints of the sUAS, and

3. Develop a data acquisition unit with digital signal processing (DSP) methods to perform direction of arrival (DOA) estimation in real-time.

1.3 Applications

The driving application for this research is the development of a prototype system that can perform direction of arrival (DOA) estimation of impulsive acoustic events while functioning onboard a VTOL sUAS. Acoustic source localization techniques have been applied for over 100 years, but the recent increase in availability of low-cost sUAS provides new opportunities. A crucial benefit that sUAS have is the ability to rapidly deploy sensors to a location in a semi-autonomous manner. SUAS also impose a unique set of constraints including a maximum payload capacity, finite power resources, and a significant amount of acoustic noise. It is the goal of this thesis to develop a proof-of-concept direction-finding module that can function reliably onboard a small unmanned aircraft vehicle (sUAV).

1.4 Literature Review

SUAS are suited for accomplishing repetitive or dangerous tasks, such as search and rescue, hazardous site inspection, real-time surveillance, monitoring agricultural fields, and many more [1]. Acoustic localization modules onboard aerial platforms have been described in the literature [2], [3], [4], and [5].

There are several acoustic DOA systems for military and law enforcement applications currently available in the US. These systems are currently only available to public entities, such as city governments, the military, and utility companies.

1.5 Contributions

This thesis has four main contributions,

1. Developed code for eight-channel synchronous sampling of the microphone sensor array,
2. Designed and fabricated a prototype direction-finding module,
3. Designed and fabricated a sUAS that hosts the microphone sensor array and system hardware, and
4. Applied DSP methods to attenuate the acoustic noise and estimate the direction of arrival.

1.6 Thesis Organization

Chapter 2 presents background information that is relevant to understanding the fundamentals of performing the objectives presented in this thesis. Chapter 3 covers the mathematical foundations and functions that are implemented in this system. Chapter 4 showcases the hardware components selected for this system and the key features of each. Chapter 5 provides an explanation of the software implemented to achieve the desired tasks. Chapter 6 presents the results and metrics of the execution and hardware assembly. Chapter 7 summarizes the accomplishments and describes future work.

CHAPTER 2: BACKGROUND INFORMATION

2.1 Small Unmanned Aircraft Vehicles

A vertical take-off and landing (VTOL) small unmanned aircraft system (sUAS) or VTOL sUAS is a specific type of UAS that can takeoff, land, and hover vertically. A sUAS is an entire flight system that includes the ground station, radio communication link, and the small unmanned aircraft vehicle (sUAV). A sUAV is defined as an aircraft controlled by a remote pilot that does not exceed 55 lb at takeoff [6]. In order to operate a sUAS for non-recreational purposes in the United States, an operator must possess a FAA part 107 remote pilot's certification with a sUAS rating [7].

SUAS are frequently referred to as drones. They have become increasingly accessible to the general public over the last few years as the price of commercially available drones has decreased to levels many can afford. Aside from the many commercial off-the-shelf ready-to-fly options, there is also a large availability of sUAS components that can be used to assemble sUAS platforms for custom applications. Considering the large amount of open-source software currently available, it is now easier than ever to develop custom built sUAS. There are many types of sUAS, including fixed-wing and multirotor variants. Although there are currently developments of VTOL fixed-wing aircraft, most VTOL sUAV are multirotors. They typically have a quadcopter or hexacopter frame, but some VTOL sUAV have up to as many as twelve motors. Due to the recent increase in availability of these VTOL sUAV, many new applications have arisen across various engineering fields. Recently low cost custom sUAS have even been used in combat, such as in Syria [8] and Ukraine [9]. These cases indicate that both military and civilians need to

be aware of the applications that sUAS potentially play a role in. SUAS are particularly useful in applications where humans cannot either safely or easily go. Some common applications of sUAS include industrial inspection, shipping and delivery, agricultural monitoring, cinematography, and defense.

2.2 Localization

The direction of arrival (DOA), also referred to as angle of arrival or direction finding, is used across many fields of engineering, including many devices that operate with frequencies throughout the electromagnetic spectrum. Sensor arrays are used for DOA estimation in fields such as seismology, radar, sonar, astronomy, and defense. It plays an important role in localization for GPS, cellular, and WIFI enabled devices. Commonly used techniques for performing DOA estimation include multiple signal classification (MUSIC), estimation of signal parameters via rotational invariance techniques (ESPRIT), maximum likelihood (ML) TDOA [10]. MUSIC and ESPRIT are frequency-based techniques that are typically used with smart antennas for beamforming and tracking of continuous signals. The TDOA technique is popular among acoustic DOA algorithms because it works well with impulsive signals and requires only passive sensors. Acoustic DOA algorithms are typically employed for speaker localization problems or for a variety of military applications. Acoustic localization for military applications has been applied since at least World War I [11]. The application was originally for detecting the location of enemy artillery locations.

2.3 Microphone Sensor Array

A microphone array is a specific type of passive sensor array comprised of passive acoustic microphones. It is a series of several microphones arranged in a known geometry. The array can be formed into either a linear two-dimensional, or three-dimensional formation. Both analog and digital microphones can be used depending on the constraints

of the engineering problem at hand. Microphone arrays are used to analyze acoustic signals. Common applications include beamforming, noise rejection, and tracking. They are most commonly used for obtaining higher fidelity signals for speech signal processing in noisy environments [12], but can also be used for military applications [13]. Rudimentary microphone arrays have been used for source localization for over one hundred years [11]. In array processing methods it is commonly assumed that the waveform, denoted by $x_i(t)$, where $i = 1, 2, ..., m$, and is observed at each node and m is the number of sensors that contains both the desired signal, denoted by $s_1(t)$, and uncorrelated noise, denoted by $n_i(t)$, which is assumed to be statistically independent between each sensor.

2.4 Time Difference of Arrival

The TDOA is one of the most commonly used methods for DOA estimation with microphone arrays. It is computationally efficient. The generalized cross-correlation (GCC) method is a very common tool used throughout the field of array processing for determining TDOA. It is an especially useful tool for direction-finding applications such as the one presented in this thesis due to its ability to calculate the time delay between two or more noisy signals [14]. The method also provides the ability to measure the similarity between two signals which is important for determining when a desired impulsive signal has occurred. The TDOA between two sensors is determined by finding the time-shift, denoted by τ, at which the cross correlation peaks.

2.5 Gunshot Acoustic Characteristics

In order to demonstrate the objective of performing acoustic direction-finding, the scope of this thesis was constrained to analyzing largely impulsive events. More specifically, the focus was on detecting and estimating the DOA of a gunshot from a firearm. Developing an understanding of the typical characteristics of gunshots was useful in making informed decisions in the data collection and post processing phases.

The explosion of a gun cartridge generates signatures in the acoustic and electromagnetic range [13]. Within the acoustic spectrum, given by 20 Hz to 20 kHz, a gunshot signature is made up of the muzzle blast and, if the bullet is supersonic, a ballistic shockwave. The generated acoustic energy is directly proportional to the volume of gas flowrate at the source and propagates at the speed of sound [15]. When sensing the acoustic wave near ground level, multipath propagation will be present. A review of these characteristics is given in the following sections.

2.5.1 Muzzle Blast

The muzzle blast is a direct result of the sudden expansion of gas immediately following the explosion inside the gun barrel [15]. The speed of sound depends on the properties of the medium through which the wave propagates. The sound pressure decreases exponentially with time, and thus the muzzle blast signal becomes sensitive to additive noise with increasing distance. Typically, a small firearm muzzle blasts a sound pulse lasting for approximately 3 ms, with a sound pressure level (SPL) of 140 dB (200 Pa) or higher [16].

2.5.2 Shockwave

A ballistic shockwave, present only when the bullet is moving at supersonic speed, is characterized by a sudden rise in pressure followed by an approximately linear decline to a value nearly as far below as the original rise and then almost instantly returns to the atmospheric pressure [17].

2.5.3 Multipath Propagation

The additive background noise and the multipath propagation effects are two common issues that cannot be overlooked in the design of acoustic localizations systems [13]. In multipath propagation environments, the received signal is composed of a direct-

path signal, which is present only when there is an unobstructed line-of-sight (LOS) from source to receiver, plus n scaled delayed copies of the direct-path signal. The scaling factor is frequency dependent and determined by the characteristics of the surface and the distance traveled, whereas the associated time-delay is determined by propagation path and the respective DOA. The multipath propagation effect poses less problems in open field and elevated environments. It is characterized by the absence of objects near the microphone array, but the analysis of recorded gunshot signals has shown that a shockwave ground reflection is almost always present [18]. In the case where the sUAS is performing DOA estimation while in flight and with a significant altitude, multipath propagation will not be significant. It may become a concern when the sUAS is operating near the ground.

CHAPTER 3: MATHEMATICAL FOUNDATIONS

3.1 Signal Model

The expected signal at the sensor can be modeled as

$$x_i(t) = s_i(t) + n_i(t), \tag{3.1}$$

where $x_i(t), s_i(t)$, and $n_i(t)$ are real, stationary random processes, and $s_i(t)$ is assumed to be uncorrelated with $n_i(t)$, $E\{s_i(t)n_i(\tau)\} = 0$ for all t,τ and $E\{n_i(t)\} = 0$ for all t, and $i = 1, 2, ..., m$.

3.2 Time Difference of Arrival

A time-based approach for DOA estimation was selected for use in this research. The delays are estimated by relating the line-of-sight (LOS) propagation distance traveled with the speed at which the signal is traveling. The set of signals of a sensor array of size m can be modeled as

$$\begin{aligned} x_1(t) &= s_1(t) + n_1(t) \\ x_2(t) &= s_1(t - D_1) + n_2(t) \\ &\vdots \\ x_m(t) &= s_1(t - D_m) + n_m(t), \end{aligned} \tag{3.2}$$

where $D_1, D_2, ..., D_m$ are the time of arrival delays between channels. The delays are to be estimated. We assume $E\{n_i(t)\} = 0$ for all i, t, and $E\{n_i(t)n_j(\tau)\} = 0$ for all i, j, t, and τ.

3.2.1 The Cross-Correlation

The cross-correlation is a well established method used in the field of digital signal processing (DSP). The continuous representation of the cross-correlation between two signals $x(t)$ and $y(t)$ is given by

$$R_{xy}(\tau) = \int_{-\infty}^{\infty} x^*(t)y(t+\tau)dt = \frac{1}{T}\int_{0}^{T} x(t)y(t+\tau)dt, \tag{3.3}$$

where T represents the observation interval and * denotes the complex conjugate. The cross-correlation of two signals $x_1(t)$ and $x_2(t)$ with zero mean additive noise is given by

$$R_{x_1x_2}(\tau) = R_{s_1s_1}(\tau + D) + R_{n_1n_2}(\tau), \tag{3.4}$$

where $\mathrm{E}\{R_{n_1n_2}(\tau)\} = 0$. Because the sUAS under investigation here is operating with digital data on an embedded system, we will implement the discrete implementation of the cross-correlation. The discrete representation of the cross-correlation between two signals $x(t)$ and $y(t)$ represented as the sequences $x[n]$ and $y[n]$, respectively, is given by

$$R_{xy}[D] = \sum_{n=-\infty}^{\infty} x^*[n]y[n+D], \tag{3.5}$$

where n represents the index of the sequence and D represents the time shift. For a sequence size of N samples and a time step of Δt, which is the inverse of the sampling frequency, the cross-correlation can be estimated as [19]

$$\hat{R}_{xy}(r\Delta t) = \frac{1}{N-r}\sum_{n=1}^{N-r} x_n y_{n+r}, \tag{3.6}$$

where the lag number is given as $r = 0, 1, 2, ..., m$, and $r\Delta t = D \approx \tau$, with $m < N$. Here, x_n is equivalent to $x[n]$ and represents the sampled value at the nth index of the signal $x(t)$.

3.2.2 Generalized Cross-Correlation with Phase Transform

The generalized cross-correlation (GCC) technique is to design filters $H_1(f)$ and $H_2(f)$ applied to the signals to provide better resolution in the time domain when estimating the TDOA between two signals [14] where f represents the frequency of interest. The role of the pre-filters is to accentuate the signal passed to the cross-correlation step at frequencies where the signal-to-noise ratio (SNR) is highest while simultaneously suppressing the noise power. These filters are implemented in the form of a weighting function $\psi_p(f)$ which is applied to whiten the input signals before performing the TDOA estimation. The performance increase is accomplished by sharpening the peak of the cross-correlation function. An example of the model can be seen in Figure 3.1.

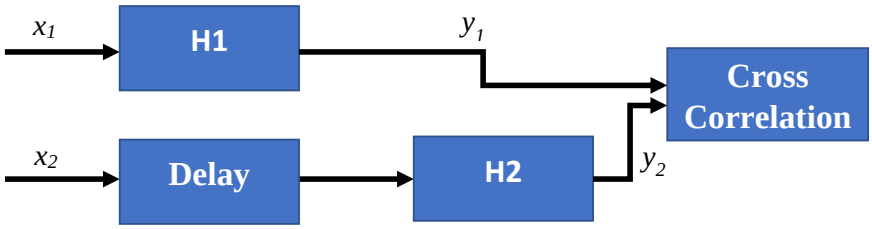

Figure 3.1: Filter Model

The GCC method with phase transform (GCC-PHAT) is a specific weighting function technique frequently used for estimating time of arrival differences in sensor networks [20], [21], [22]. The GCC-PHAT method normalizes the signal cross-spectral density by the spectrum magnitude. The cross-spectral density or cross-power spectrum is given by taking the Fourier transform of the cross correlation, or

$$S_{y_1y_2}(f) = \int_{-\infty}^{\infty} R_{y_1y_2}(\tau) e^{-j2\pi f\tau} d\tau. \tag{3.7}$$

The signals $y_1(t)$ and $y_2(t)$ correspond to $x_1(t)$ and $x_2(t)$, respectively, after the filters are applied. The cross-power spectrum for the model in Figure 3.1 can be represented as

$$S_{y_1y_2}(f) = H_1(f){H_2}^*(f)S_{x_1x_2}(f), \tag{3.8}$$

The filters $H_1(f)$ and $H_2(f)$ can be related to the weighting function for the GCC-PHAT method by

$$\psi_p(f) = \frac{1}{|S_{x_1x_2}(f)|} = H_1(f)H_2^*(f). \tag{3.9}$$

These computations are accomplished for each combination of sensors in the sensor array. A new estimate for the TDOA between two channels can be found by taking the inverse Fourier transform of the estimated cross-power spectrum with the weighting function applied, yielding

$$\hat{R}_{y_1y_2}(\tau) = \int_{-\infty}^{\infty} \psi_p(f)\hat{S}_{x_1x_2}(f)e^{j2\pi f\tau}df. \tag{3.10}$$

This method can be used to solve for an estimate between two discrete signal sequences of different lengths. For example, let N be the number of elements in the sequence $y_1[n]$ and M be the number of elements in the sequence $y_2[m]$ assuming the elements outside of the sequence size are equal to zero. A sequence of cross-correlation coefficients with negative indexing $\mathbf{h} \in \mathbf{R}^{(N+M-1)\times 1}$ can be found. For the indexes of

$$j = -(N-1), -(N-2), ..., -1, 0, 1, ..., (M-2), (M-1), \tag{3.11}$$

the cross-correlation coefficient can be obtained for each index in $\mathbf{h}$ by

$$h_j = \sum_{b=0}^{N-1} y_{1b}y_{2_{j+b}}. \tag{3.12}$$

The elements of the cross-correlation sequence $\hat{\mathbf{R}}_{y_1y_2}$ between the two signals are related to the elements in $\mathbf{h}$ by

$$\hat{R}_{y_1y_{2_i}} = h_{i-(N-1)} \tag{3.13}$$

for the index

$$i = 0, 1, 2, ..., N + M - 2. \tag{3.14}$$

The TDOA between the two signals can be estimated by finding the maximum value from the sequence $\hat{R}_{y_1y_2}(\tau)$, or

$$\hat{\tau}_{y_1y_2} = \underset{\tau}{\operatorname{argmax}}\, \hat{\mathbf{R}}_{y_1y_2}(\tau) \tag{3.15}$$

The estimate of time delay between the two channels $\hat{\tau}_{y_1y_2}$ is calculated by finding the index of the maximum value in the sequence, accounting for the shift $(N-1)$, and multiplying by the sampling period Δt, yielding

$$\hat{\tau}_{y_1y_2} = (i - (N-1)) \times \Delta t. \tag{3.16}$$

3.3 Direction of Arrival

The DOA algorithm selected for this application was chosen from [23]. The approach was selected because it could be easily adopted to perform with any arbitrary array geometry where all of the relative microphone positions are known. Because the distance between any two omnidirectional microphones in the sensor is small relative to the acoustic source, it is assumed that the wave front propagates as a plane which leads to a set of linear equations [10]. The time delay with which the LOS signal arrives at each microphone is estimated and used to make an estimate for the DOA. First an initial estimate of

DOA is determined from a closed form solution to the linear least squares problem. This estimate can then used as a reference to begin the search for a solution to a non-linear least squares problem. The non-linear least squares approach was modeled in MATLAB with simulated data, but it was not employed on the real-time system due to timing constraints. For a microphone sensor array, the position of the *ith* sensor can be given as

$$\mathbf{P}_i = \begin{bmatrix} x_i \\ y_i \\ z_i \end{bmatrix}, \tag{3.17}$$

where $\mathbf{P}_i$ is defined with respect to a given reference. In this case, the microphone array was designed with spherical geometry so that there is a central origin. The origin of the array is fixed in place onboard the sUAV frame so that it can be referenced relative to the autopilot and GPS. The DOA of the acoustic event of particular interest can be represented as a three-component vector, originating from the aforementioned origin, defined by the azimuth and elevation angles, ϕ and θ, respectively, as

$$\mathbf{K} = \begin{bmatrix} k_x \\ k_y \\ k_z \end{bmatrix} = \begin{bmatrix} \sin\theta\cos\phi \\ \sin\theta\sin\phi \\ \cos\theta \end{bmatrix}. \tag{3.18}$$

Using the known positions of two microphones, denoted by i and j, we can relate this to the TDOA between two channels as

$$\tau_{i,j} = \frac{1}{c}\Big[(x_j - x_i)\sin\theta\cos\phi + (y_j - y_i)\sin\theta\sin\phi + (z_j - z_i)\cos\theta\Big], \tag{3.19}$$

where c is the speed of sound in air. This definition can be related to the DOA vector $\mathbf{K}$ and the position vectors $\mathbf{P}_i$ and $\mathbf{P}_j$ by taking their differences projected onto the DOA

vector, yielding

$$\tau_{i,j} = \frac{1}{c}[\mathbf{P_j} - \mathbf{P_i}]\mathbf{K}. \tag{3.20}$$

The reference-free approach is chosen in order to employ the full set of TDOA measurements. We form the reference-free position difference matrix $\mathbf{S}$ by calculating the position difference between each combination of microphones in the array where N is the number of sensors in the array

$$\mathbf{S} = [\mathbf{P}_2 - \mathbf{P}_1, ..., \mathbf{P}_N - \mathbf{P}_1, \mathbf{P}_3 - \mathbf{P}_2, ..., \mathbf{P}_N - \mathbf{P}_{N-1}]^T \in \mathbf{R}^{\frac{N(N-1)}{2} \times 3}. \tag{3.21}$$

A reference-free TDOA vector $\hat{\boldsymbol{\tau}}$ can be formed by placing the TDOA between all combinations of microphones in the array as follows,

$$\hat{\boldsymbol{\tau}} = [\tau_{2,1}, ..., \tau_{N,1}, \tau_{3,2}, ..., \tau_{N,2}, ..., \tau_{N,N-1}]^T \in \mathbf{R}^{\frac{N(N-1)}{2} \times 1}. \tag{3.22}$$

This leads to a set of linear equations of the form

$$\hat{\boldsymbol{\tau}} = \frac{1}{\hat{c}}\mathbf{S}\hat{\mathbf{K}}, \tag{3.23}$$

where the estimate of the speed of sound is represented as $\hat{c}$. The least squares cost function is defined as

$$l(\hat{\mathbf{K}}) = \left\| \hat{\boldsymbol{\tau}} - \frac{1}{\hat{c}}\mathbf{S}\hat{\mathbf{K}} \right\|^2, \tag{3.24}$$

where $\|\cdot\|$ denotes the standard Euclidean norm. A closed form linear least squares solution to the DOA vector is given by

$$\hat{\mathbf{K}} = -\hat{c}(\mathbf{S}^T\mathbf{S})^{-1}\mathbf{S}^T\hat{\boldsymbol{\tau}}. \tag{3.25}$$

Utilizing the components from the DOA vector $\hat{\mathbf{K}}$, we can solve for the azimuth angle as

$$\hat{\phi} = \tan^{-1}\Big(\frac{\hat{k}_y}{\hat{k}_x}\Big), \tag{3.26}$$

and the elevation angle as

$$\hat{\theta} = \tan^{-1}\Big(\frac{\sqrt{\hat{k}_x^2 + \hat{k}_y^2}}{\hat{k}_z}\Big). \tag{3.27}$$

CHAPTER 4: HARDWARE

4.1 sUAS Design

The critical subsystems and components of the sUAS along with some of the key parameters include:

1. sUAV Frame
2. Powertrain
3. Pixhawk 2.1 Autopilot
4. Radio Control and Telemetry
5. HERE Global Navigation Satellite System (GNSS)

4.1.1 sUAV Frame

The sUAV frame is an all carbon fiber frame except for the assembly hardware, motor mounts and boom blocks [24]. It is a hexacopter layout with a boom radius of approximately 12.5 in., as depicted in Figure 4.1. A hexacopter layout was selected because it could provide both a functional payload capacity and a more stable flight when compared to a quadcopter. The Turnigy Talon V(1.0) frame was selected due to its lightweight and minimalist footprint which allows for customization of the platform.

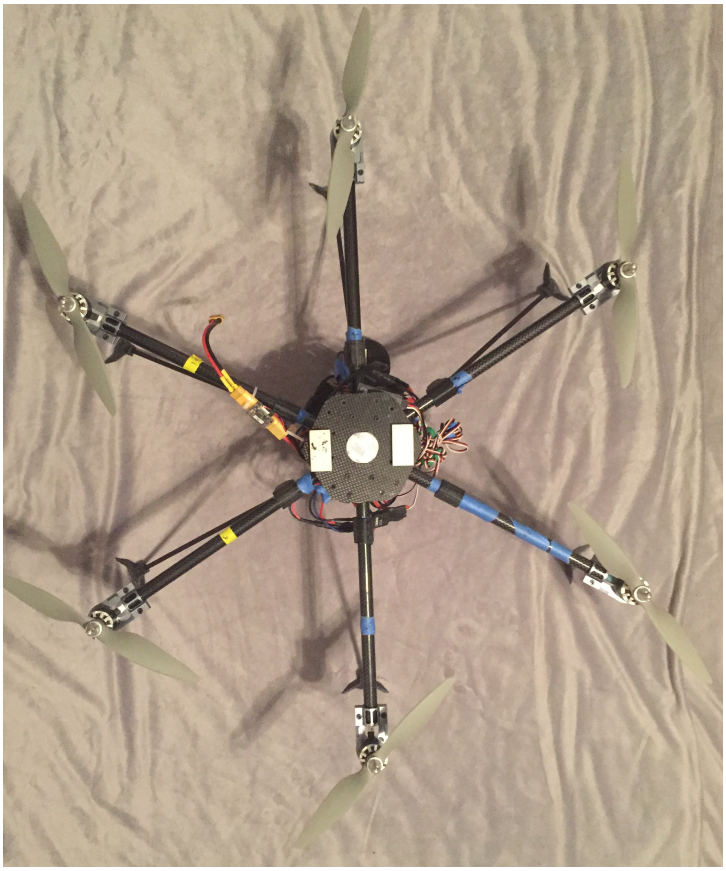

Figure 4.1: sUAV Hexacopter Frame

4.1.2 Powertrain

The motors selected for this project were the KDE 2315XF-2050, as shown in Figure 4.2. This selection is a brushless motor designed specifically for multi-rotor use. The key motor parameters from [25] can be seen in Table 4.1.

Figure 4.2: KDE 2315XF-2050 Motor

Table 4.1: Key Motor Specifications

Component	**Spec.**
K_v (Motor Velocity Constant)	2,050 RPM/V
K_t (Motor Torque Constant)	0.0047 N-m/A
K_m (Motor Constant)	0.0253 N-m/$\sqrt{W}$
I_0 (@10V)	1.3A
ESC PWM Rating	16-32kHz
Weight	64 g
Peak Thrust	2220g

The electronic speed controller (ESC) selected was the Arris 30A brushless ESC that supports use with 2S-6S cell lithium polymer batteries as shown in Figure 4.3. There is a 3-pin signal connection directly to the autopilot, power, and ground connected to the power distribution board and three banana plugs for rotational-direction free control to the motors [26]. The Arris 30A ESC supports a continuous current of 30A and a maximum burst current of 45A. The ESCs come pre-wired, so it is only required to solder the exposed wires to a board or use bullet connectors.

Figure 4.3: 30A Electronic Speed Controller (ESC)

The battery chosen for this platform is the Storm 14.8V lithium-polymer 4 cell battery, shown in Figure 4.4 [27]. It has a capacity of 4000mAh.

Figure 4.4: 4000mAh Battery

The propellers selected are the Raycorp 9045 manufactured of glass-fiber reinforced nylon [28]. They have a diameter of 9 in. and a pitch of 4.5 in. The pitch is defined as the distance the propeller would move forward under a no-slip condition and is a contributing factor for the amount of torque generated. These propellers, shown in Figure 4.5, are slightly larger than the ideal size for the selected motors, but were chosen based on their availability and low cost.

Figure 4.5: 9x4.5 Propeller

The power distribution board (PDB) selected from Matek Systems is shown in Figure 4.6. It has a single XT60 connector for power directly from the battery and solder pads for 6 motors. It supports 3S-4S cell batteries between 9V and 18V and includes 5V and 12V DC output to power additional peripherals [29]. This is a convenient lightweight PDB with built in power LED indicators.

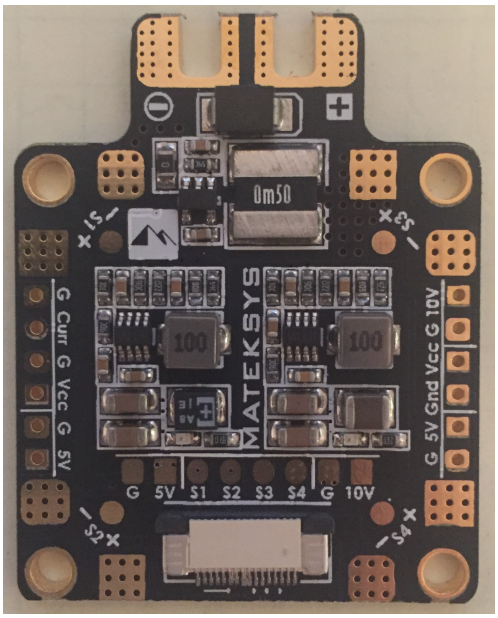

Figure 4.6: Power Distribution Board

The power module, shown in Figure 4.7, is packaged with the the Pixhawk 2.1. It has XT-60 connectors for receiving power directly from the battery along with the required 5V output to the Pixhawk in a 6 wire configuration [30].

Figure 4.7: Power Module

4.1.3 Autopilot

The Pixhawk, shown in Figure 4.8, is a very common autopilot known for its reliability and large user base. It is an open-source hardware project designed to run seamlessly with the open-source software PX4 on the NuttX operating system [31]. The system provides a variety of digital protocol ports including an Intel Edison port for additional computing power. The Cube is a sensor system connected to the board that includes vi-

bration isolation on two of the inertial measurement units (IMUs) and a third IMU as a backup/reference. The key Pixhawk features are described in Table 4.2.

Figure 4.8: Pixhawk 2.1

Table 4.2: Key Pixhawk Specifications

32 bit STM32F427 Cortex Core
168 MHz Processor
256 KB RAM
32 MB Flash Memory
14 PWM Servo Outputs
UART, I2C, CAN connections
Multi-tone Audio Indicator
Multicolor LED Indicator
Redundant Power Supply Inputs
MicroSD Slot for Data Logging
3 Accelerometers
3 Gyroscopes
3 Magnetometers
2 Barometers

4.1.4 Radio Control and Telemetry

The FrSKY Taranis QX7, shown in Figure 4.9, was selected as the transmitter. It can control up to 16 separate channels and operates on open source firmware OpenTX [32]. It has an LED backlit screen with a retrieval signal strength indicator (RSSI). Flight data logs are saved in real-time directly to an onboard microSD card. It has audio speech outputs, haptic vibration feedback, and quad ball bearing gimbals.

Figure 4.9: Taranis QX7 Transmitter

The RF receiver chosen is the FrSKY X8R, shown in Figure 4.10. It is developed to work seamlessly with the selected transmitter. It supports 8 channels and can be used in combination with another X8R to control up to 16 servo channels through the SmartPort [33]. The SmartPort (or S.Bus) is a 3 wire configuration with a protocol that operates in full duplex. It functions with either 6 AA batteries or a rechargeable lithium battery.

4.1.5 GPS

The GPS selected was the HERE GNSS, shown in Figure 4.11, which was released along with the Pixhawk 2.1. It provides concurrent reception of up to 3 global GNSS with

Figure 4.10: FrSKY X8R 2.4GHz Receiver

167 dBm sensitivity [34]. This includes reception of GPS, Galileo, GLONASS, and Bediou for autonomous geo-spatial positioning with global coverage.

Figure 4.11: HERE Solo GPS Module

4.2 Localization Module

The localization module includes all of the hardware required to perform data aquisition and DOA estimation. It is a standalone system that could function independently or while deployed onboard the sUAV. The components include:

1. Omnidirectional Microphone
2. Microphone Sensor Array Frame
3. Texas Instruments ADS1278 EVM-PDK

4. National Instruments myRIO

5. Custom Designed Interface PCB

4.2.1 Microphone Selection

The microphone is an omnidirectional analog micro electro-mechanical system (MEMS) shown in Figure 4.12 that is produced as a breakout board with an operational amplifier [35]. This selection was made because it is embedded in a pre-amplifier circuit with a small foot print. It is a very lightweight and low-cost selection. The MEMS configuration was chosen over electret condenser types due to its resiliency to mechanical vibration. The microphone itself has a frequency range of 100Hz-10kHz with a sensitivity of 42dB $\pm 3dB$ @ 94dB SPL and a SNR of 59 dB [36]. The breakout requires 3.3V, ground, and a single ended audio signal wire [35]. The board has an approximate DC bias of 0.7V and a typical response around 100mV peak-to-peak with noise near the microphone. It can amplify signals to a maximum of 1V peak-to-peak.

Figure 4.12: Adafruit Silicon MEMS Microphone Breakout-SPW2430

4.2.2 Array Design

The microphone array is spherical in shape as illustrated in Figure 4.13, and was assembled out of 0.3 in. carbon fiber tubes and a custom designed frame. There are eight

Figure 4.13: 8 Channel Microphone Array Design

microphones placed at each of the ends of the 11.25 in. tubes. The frame was modeled in SolidWorks and 3D printed out of polylactic acid (PLA). The custom fabrication of the array allowed for weight and layout optimization that addressed the constraints from the sUAV. The 3 wires required for each microphone baord are housed inside the carbon fiber tubing. The set of wires is joined into a single 24 pin female connector for quick connect and disconnect from the interface board.

4.2.3 TI ADS1278 EVM-PDK

The TI ADS1278 evaluation module product demonstration kit (EVM-PDK), shown in Figure 4.14, is an evaluation board for TI's synchronous, 24 bit, 8-channel, delta-sigma, analog-to-digital converter (ADC), the ADS1278 [37]. The board provides a quick path to prototyping using the ADC because it contains all the support circuitry needed to connect the ADC with an embedded system [38]. It was selected specifically because of its ability to sample multiple analog channels synchronously. The board requires 1.8V, 3.3V, and 9V power supplies in order to operate. The board has switches onboard that allow the user

to define modes of operation, such as low-power, high-speed, and high-resolution. Some of the key features of the EVM-PDK are described in Table 4.3.

Table 4.3: Key ADS1278 EVM-PDK Specifications

SPI Output
27 MHz Onboard Oscillator
Accepts External Modulator Clock
User-defined Sampling Rates
Maximum Data Rate of 144 kSPS per Channel
Built in Anti-Aliasing Filter Circuitry
Linear Phase Digital Filter
Maximum 111dB SNR
-108dB Total Harmonic Distortion

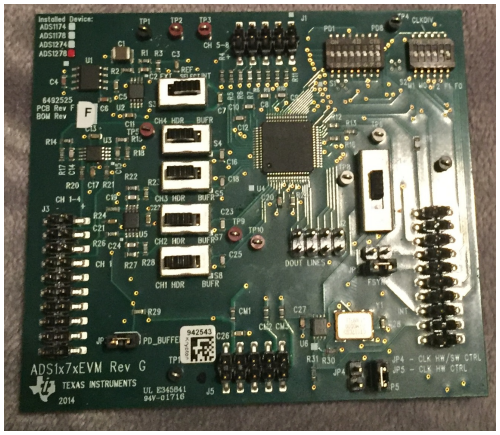

Figure 4.14: ADS1278 EVM-PDK ADC

4.2.4 NI myRIO

The National Instruments myRIO, shown in Figure 4.15, was selected to perform the real-time computations. It is an embedded system with a Xilinx Z-7010 field programmable gate array (FPGA) as well as a dual-core ARM Cortex-A9 central processing unit (CPU) [39]. The key features of the myRIO can be seen in Table 4.4.

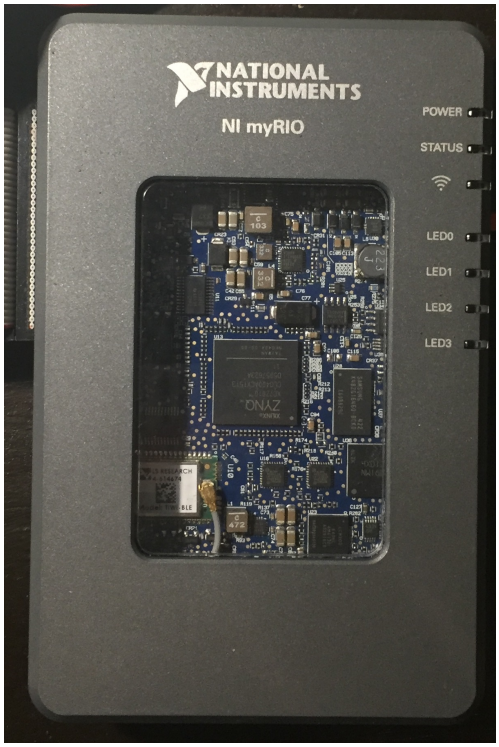

Figure 4.15: National Instruments myRIO Embedded System

Table 4.4: Key myRIO Specifications

667 MHz Processor Speed
256 MB of DDR3 Memory
40 MHz onboard Oscillator
Onboard 3-axis Accelerometer
40 digital I/O lines
6V to 16V Power Supply
WIFI enabled
Programmable with LabVIEW, C, and Python

The ability to develop functioning FPGA code with LabVIEW is a crucial benefit that the myRIO provides. The FPGA was leveraged to execute the high rates of data processing with hardware-timed speed and reliability.

4.2.5 Interface Board

The interface board, shown in Figure 4.16, is a custom designed and fabricated modular 2-layer printed circuit board (PCB) that functions as an interface between the myRIO, ADS1278 EVM-PDK, and the microphone array. It was designed according to the parameters provided from [40]. The board stacks directly on top of the ADS1278 EVM-PDK and provides one 34 pin header for the myRIO and another 24 pin header for the microphone array. 5V and 3.3V power are supplied directly from the myRIO where they are dispersed to the required locations. Each microphone board receives 3.3V, the ADS1278 EVM-PDK receives 3.3V and 5V as well as 1.8V which is supplied via a low dropout linear voltage regulator [41] on the board itself.

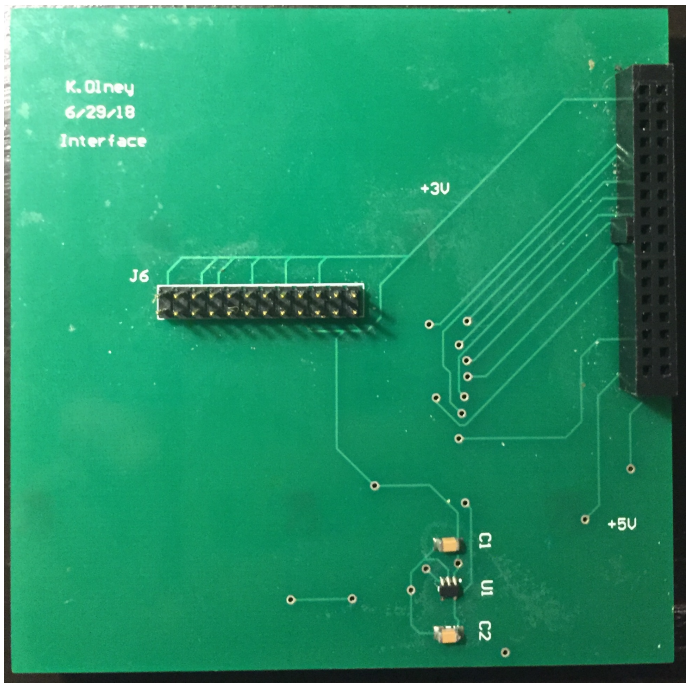

Figure 4.16: Top of Interface Board with 34 and 24 Pin Headers

CHAPTER 5: SOFTWARE

A general overview of the data processing is shown in Figure 5.1. Analog data is received and amplified at each sensor of the microphone array. The analog data is then digitized and sent to the FPGA on the myRIO via a serial peripheral (SPI) bus for pre-processing. After pre-processing, the data is transferred to the CPU via a direct memory access (DMA) first-in, first-out (FIFO) where the real-time digital signal processing and direction of arrival estimation are performed.

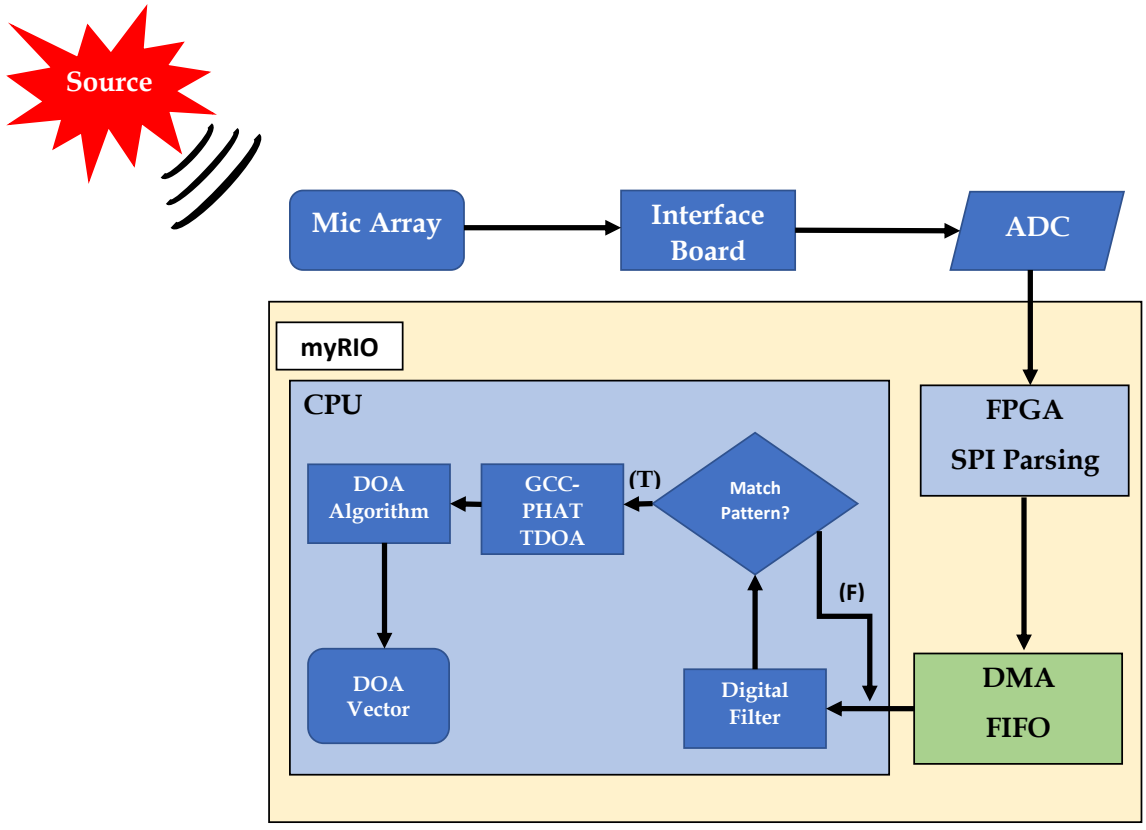

Figure 5.1: Overview of Data Flow

5.1 FPGA Implementation

The benefit of reconfigurable I/O (RIO) FPGA architecture is that each channel of data can be transfered through an independent digital line in the form of 24 bit 2's complement.The top level of the FPGA code is shown in Figure 5.2. The data is being received at 93.75 kSPS per channel. The FPGA code is executed within a single-cycle timed loop (SCTL) operating at 48 MHz. The SCTL functions as a state machine that depends on the status of the serial peripheral interface (SPI) bus. When data is ready, a digital pin toggles high to enable the parsing of data on the FPGA. The data is converted to a signed 32 bit integer before it is placed into an array and sent to a local FIFO. The local FIFO is used to transfer the data outside of the SCTL and is necessary because an array of data cannot be written to a DMA FIFO inside a SCTL. The array of 8 channels of synchronously sampled data is sent to a DMA FIFO so it can be read by the CPU.

5.2 CPU Implementation

The code deployed on the CPU is the top level virtual instrument (VI) of the application. Configuration is first required to enable the FPGA code and to initialize the DMA FIFO. The top level, shown in Figure 5.3, functions with a producer-consumer loop format. A user-defined control is determines the frame size of the data read from the DMA FIFO.

5.2.1 Noise Rejection

Aside from the pre-whitening filter applied for the GCC-PHAT method, different digital filters were explored to address the noise generated from the propellers of the sUAS. Based on the understanding that the peak energy of the drone noise generally falls between 500 and 1.8kHz, a bandstop filter was applied with these bounds. This is a single

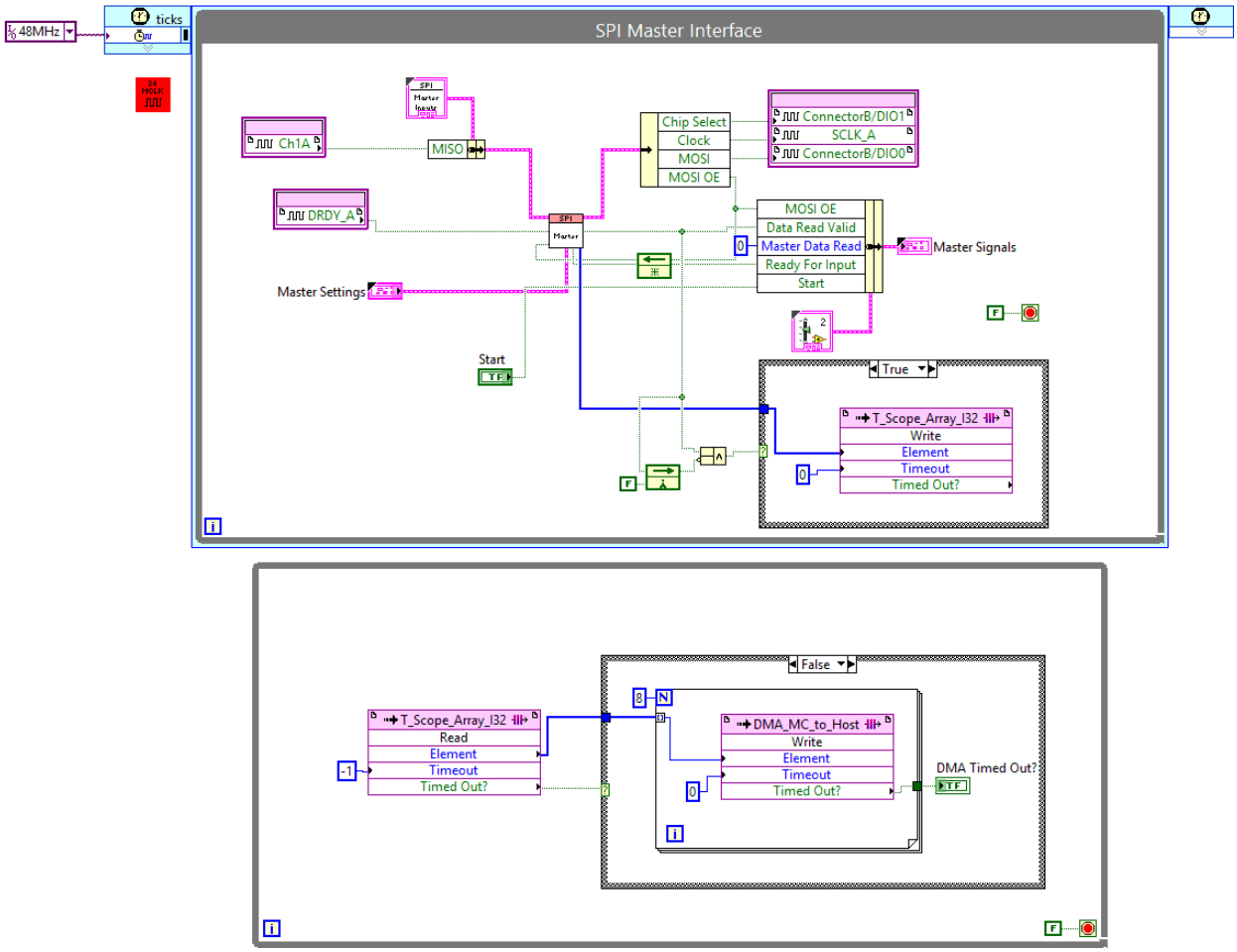

Figure 5.2: Top Level of FPGA Code

digital FIR filter applied to the single channel used for detecting significant impulsive sounds.

5.2.2 Impulse Detection

A simple cross-correlation is applied between the wavelet of a single channel and a template of a gunshot impulse to detect when a significant event has occurred. The cross-correlation is applied to the first channel of every frame of data read in the producer loop. The maximum value of the cross correlation between the two signals is compared to a threshold value that is user-defined. When the maximum of the cross-correlation function

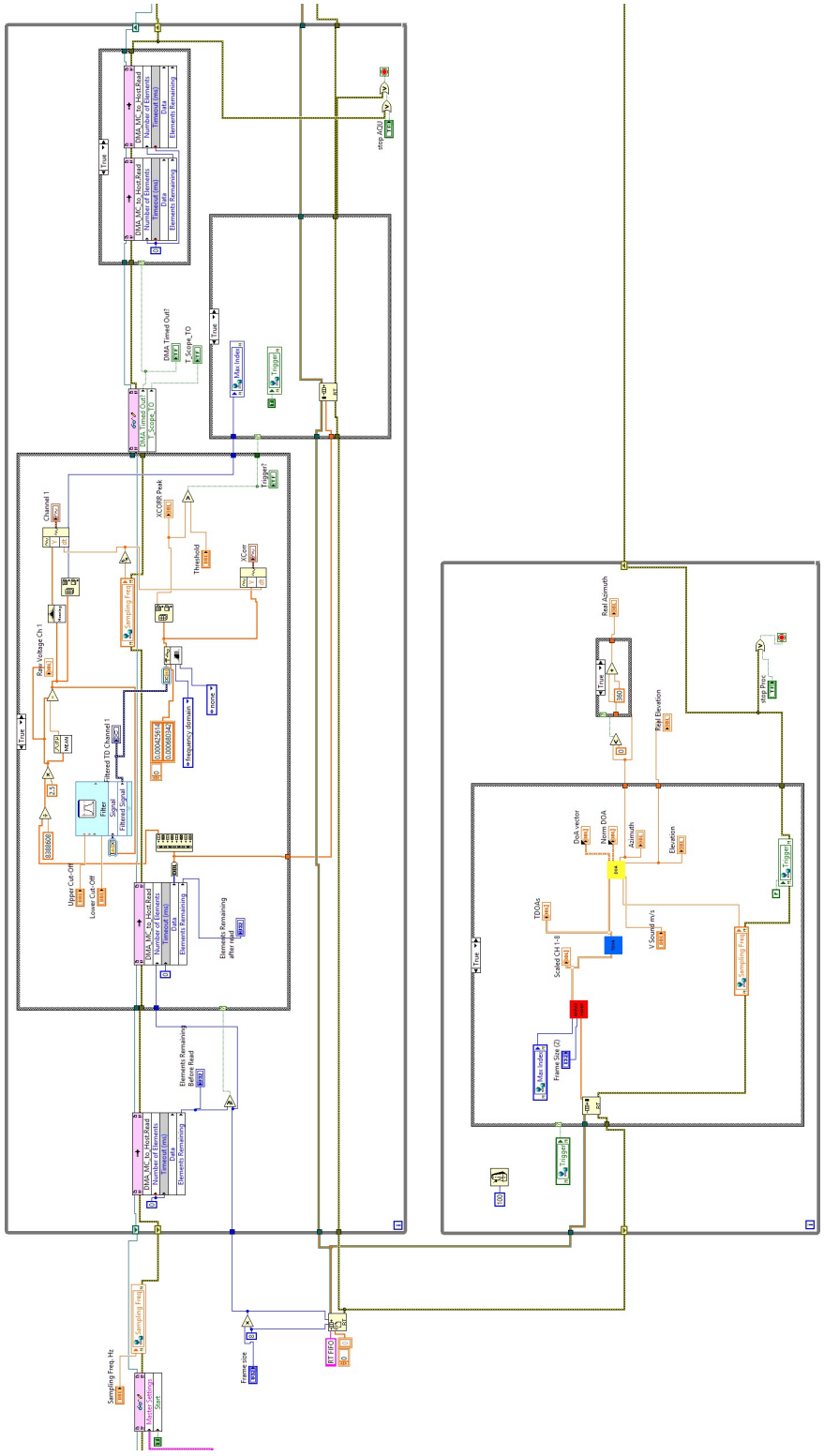

Figure 5.3: Top Level of CPU Code

exceeds the threshold, then it is assumed there is a waveform match which triggers the next loop for processing.

5.2.3 DOA Estimation

When the impulsive noise is detected, all of the data read from the DMA FIFO is sent to separate loop to perform the DOA estimation. This consumer loop estimates the TDOA for all combinations of channels before estimating the DOA.

CHAPTER 6: RESULTS

6.1 Data Collection

In order to evaluate the system's ability to detect and estimate DOA of an impulsive acoustic event, different gunshots were recorded at an outdoor shooting range. This included a variety of nine distinct handgun and rifle calibers. Data was sampled at a rate of 93.75kHz and at a distance of approximately twenty-nine feet away from the shooter location. In this first stage of the experiment, five recordings of each caliber were made with minimal ambient noise. This was done so that the distinct signature for each caliber could be isolated for further analysis. In the second stage of the experiment, the same procedure from the first phase was followed except that the sUAS motors were operating so that recordings could be made with the additional noise generated from the propellers.

In both cases, the sUAV was stationed at ground level. For the second stage, the propellers were flipped upside down due to the fact that the sUAV had not been reliably flown at the time. This modification, which generated thrust in the downward direction, allowed for the propeller noise to be generated without the threat of a catastrophic crash. Isolated recordings were made with the motors operating at various throttle positions before recording the gunshots with the additive noise from the propellers.

6.2 Acoustic Signal Analysis

Post-processing of the recorded data was completed in order to determine the typical acoustic characteristics of the sUAV under operation as well as the acoustic characteristics of different gunshot calibers. After exploring the signals in both the time and frequency

domains, a digital filter was selected that could mitigate the influence of the propeller noise while preserving the time-domain response of the gunshot muzzle blast.

6.2.1 Time Domain Characteristics

The raw noise generated by the propellers can be observed in Figure 6.1 where all eight channels are plotted. The generated noise has a magnitude of ≈ 20 mV peak-to-peak. The raw signals are plotted with their DC bias which is unique for each microphone due to the pre-amplifier.

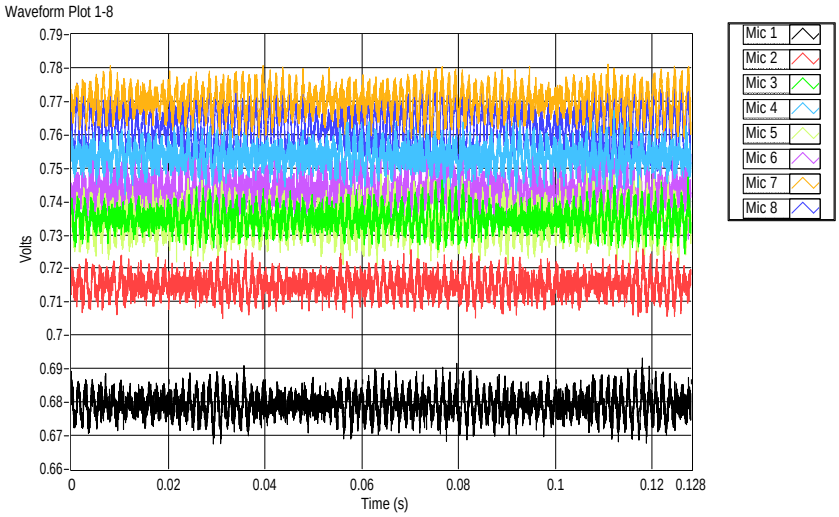

Figure 6.1: 8 Channels of Propellers Operating at 50% Throttle

A recording of an isolated 9mm handgun (Glock 19) muzzle blast can be seen in Figure 6.2 which is characterized by a large initial impulse followed by a quick decay. The raw voltage is plotted with the total length of the recorded impulsive event is approximately 3ms which is in agreement with [42]. The DC bias is removed in this representation, so that the raw signal magnitude of approximately 0.07V peak-to-peak can be observed. In Figure 6.3 the plots of raw data of two synchronously sampled channels can be observed with the same 9mm muzzle blast from figure F.2.

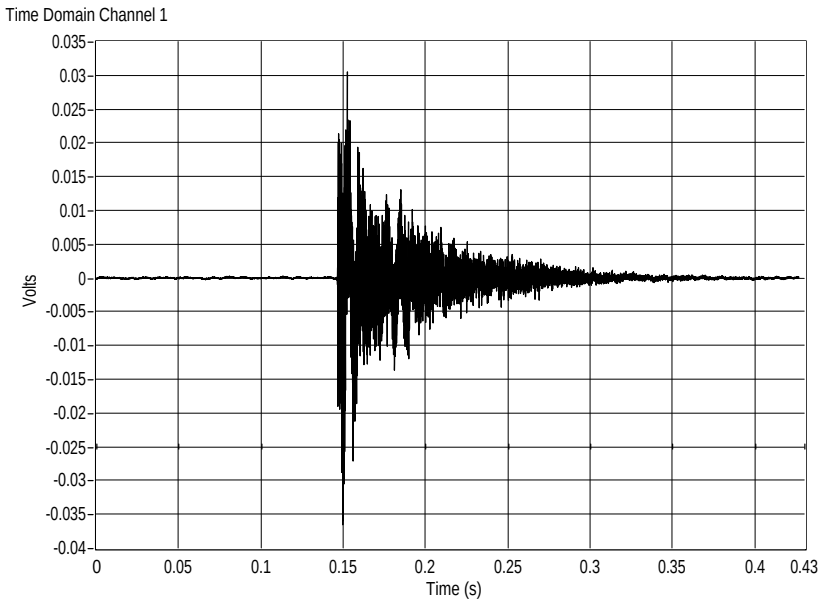

Figure 6.2: Raw 9mm Gunshot

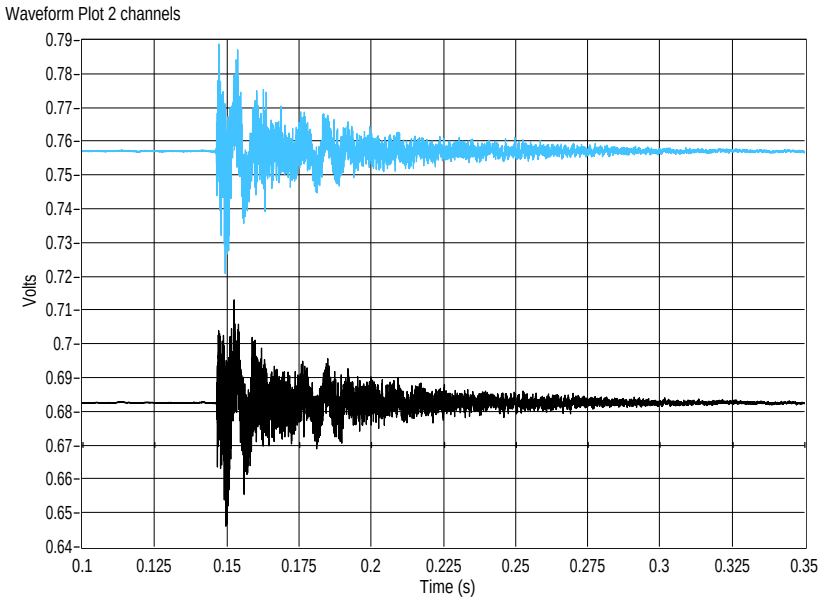

Figure 6.3: Raw Two Chanel 9mm Muzzle Blast Recording

The raw data of a 9mm gunshot recorded with the additive noise generated from the propellers rotating, shown in Figure 6.4, illustrates the significant amount of noise present, but there is clearly some impulsive noise observed.

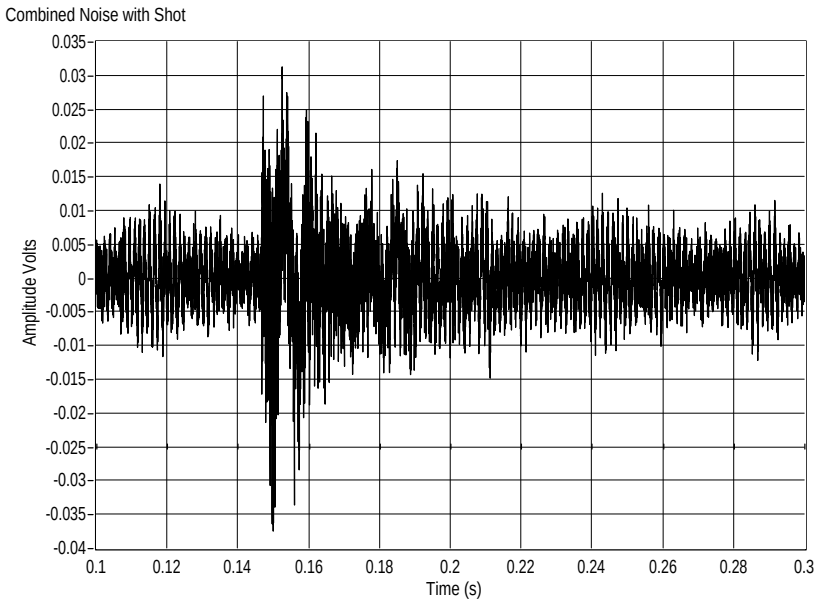

Figure 6.4: Unfiltered Propeller Noise with Gunshot

6.2.2 Frequency Characteristics

After analyzing the noise present while the sUAS had its motors operating, it was shown that the frequencies generated by the propellers mostly fell between 500 Hz and 800 Hz throughout the throttle range. The normalized fast Fourier transform (FFT) of a single channel with the propellers operating at 50% throttle is shown in Figure 6.5.

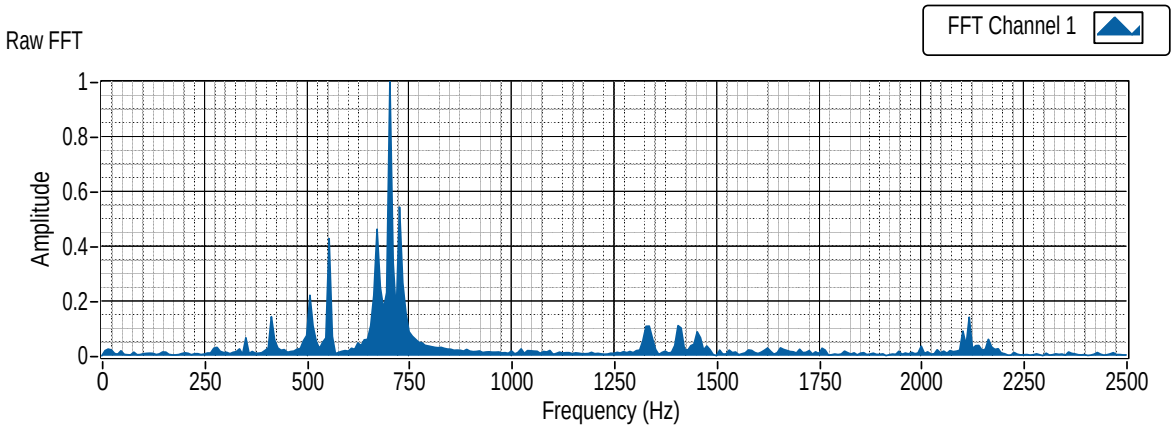

Figure 6.5: FFT of Single Channel Propeller Noise

The normalized frequency response of an isolated 9mm muzzle blast can be observed with a frequency band from 0 Hz to 600 Hz in Figure 6.6. The most significant portion

of the frequency content is below 250 Hz. The frequency content of the gunshot falls just below the lowest frequency of interest from Figure 6.5.

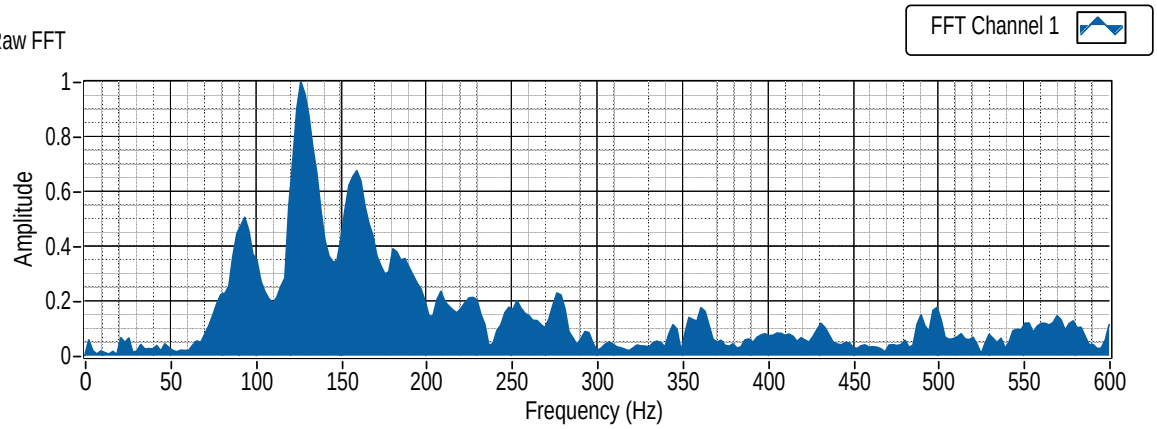

Figure 6.6: Lower Band FFT of 9mm Gunshot

6.2.3 Applied Filtering

Based on the preceding analysis of frequency content present in the system, a variety of static digital finite impulse response (FIR) filters were tested in order to minimize the affects of the propeller noise. A low-pass filter with a cutoff frequency of 300 Hz was shown to work well at minimizing propeller noise while preserving the time domain response of the muzzle blast. The magnitude response of the selected 511 taps FIR filter can be seen in Figure 6.7. A benefit of the application of an FIR filter is the linear phase response which can be observed in Figure 6.8

The FFT of the propeller noise after filtering can be see in Figure 6.9. The frequency plot was normalized with respect to peak response from Figure 6.5. The FIR filter works well at attenuating frequencies present when the motors are operating.

The implementation of the filter on the isolated 9mm gunshot, shown in Figure 6.10, accomplishes the desired result by removing the undesirable frequency content. In Figure 6.11 four synchronously sampled channels of a 9mm gunshot recording with the filter applied to all channels are plotted. Cursors are shown at the peaks of channel 3 and

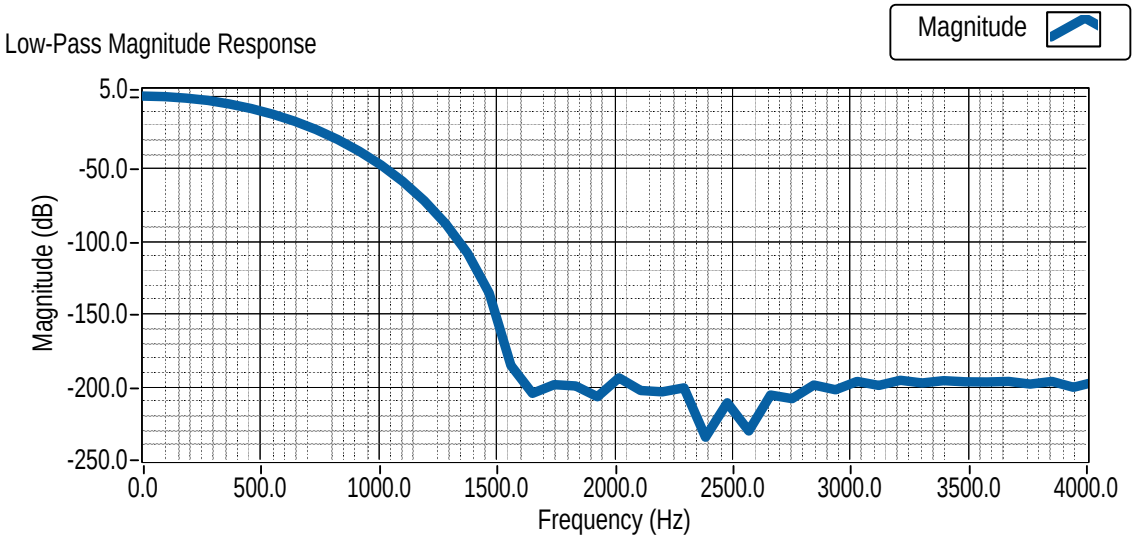

Figure 6.7: Magnitude Response of Low-Pass FIR Filter

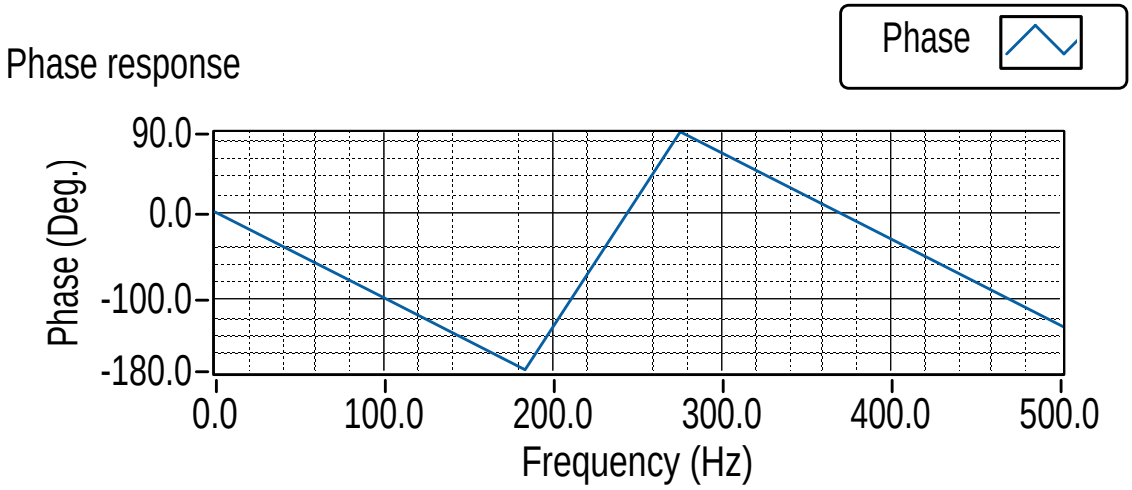

Figure 6.8: Phase Response of Low-Pass FIR Filter

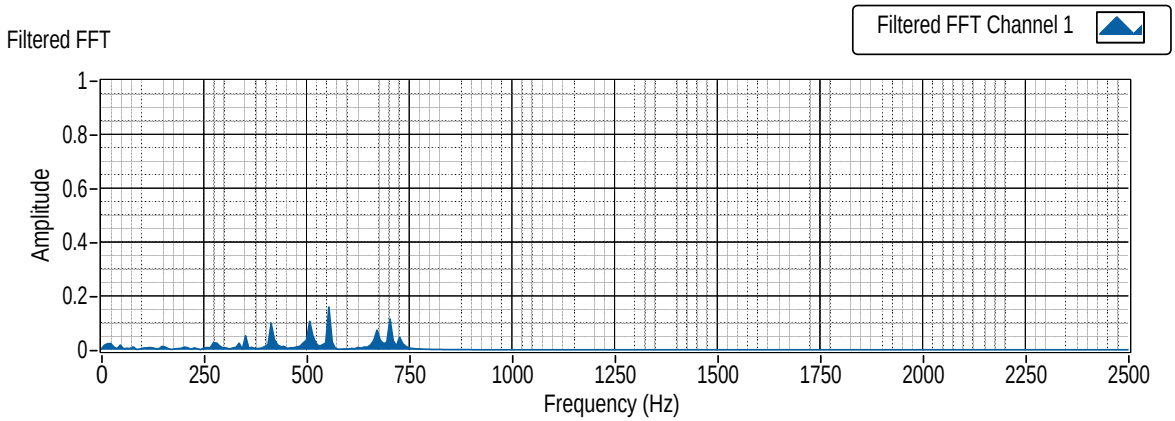

Figure 6.9: FFT of Filtered Single Channel Propeller Noise

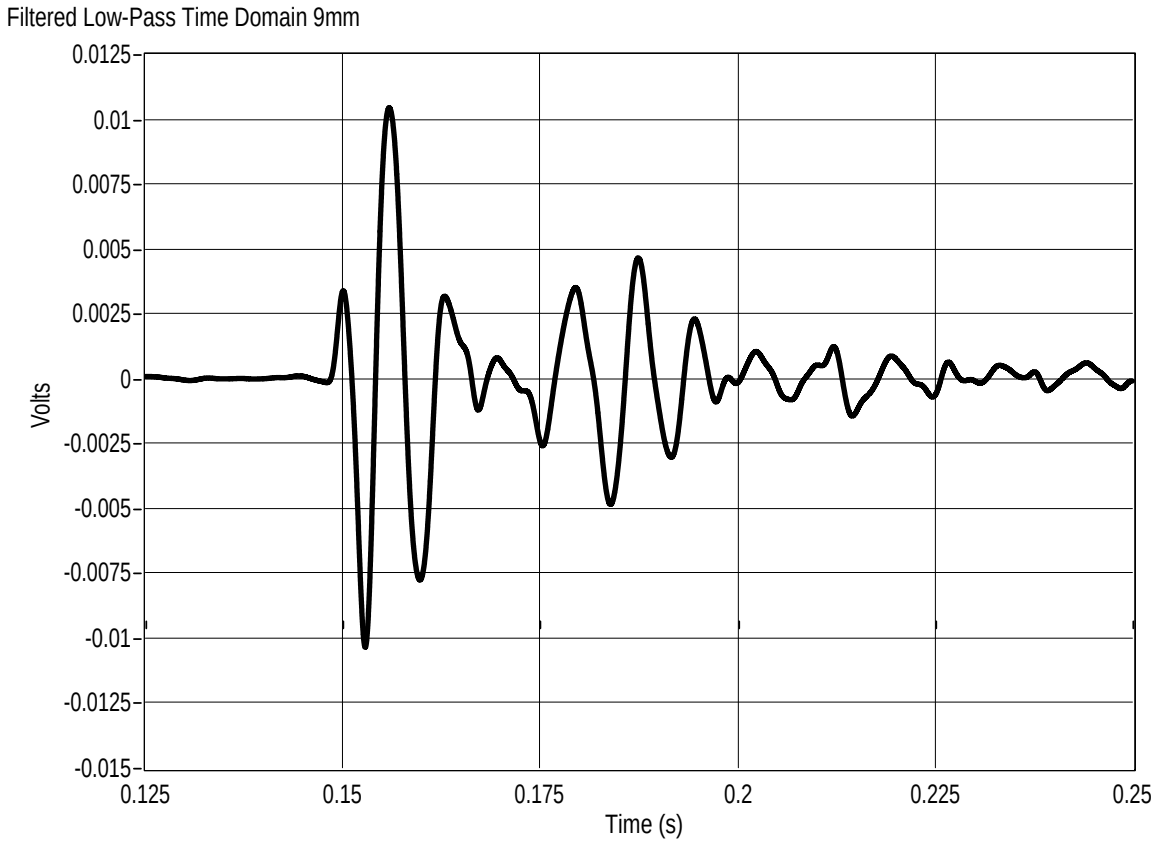

Figure 6.10: Filtered Time Domain Representation of 9mm Recording

channel 4 so that an observation of the TDOA of approximately 0.5ms can be observed. When the filter is applied to the same signal from Figure 6.4, where both a 9mm gunshot is present with additive propeller noise, the propeller noise is successfully removed while the gunshot blast is preserved. This is shown in Figure 6.12.

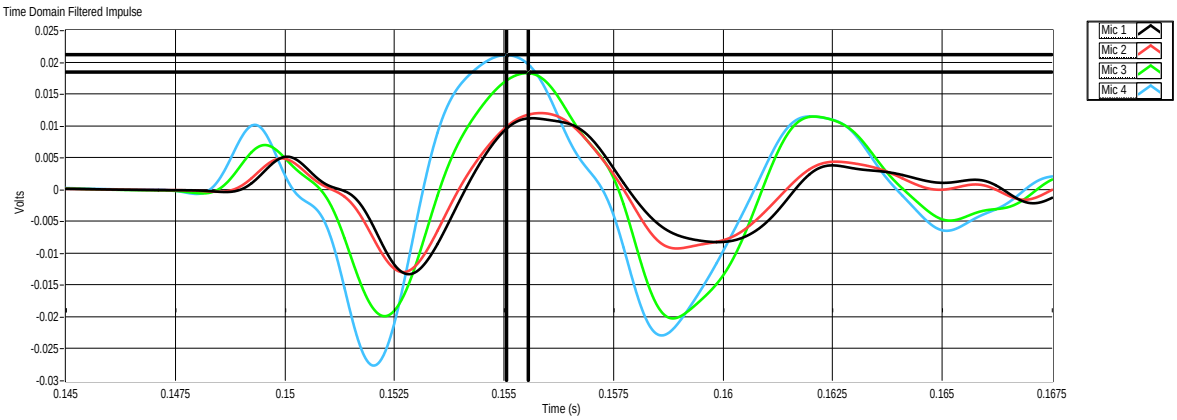

Figure 6.11: Synchronous Plot of 4 Filtered Channels (9mm)

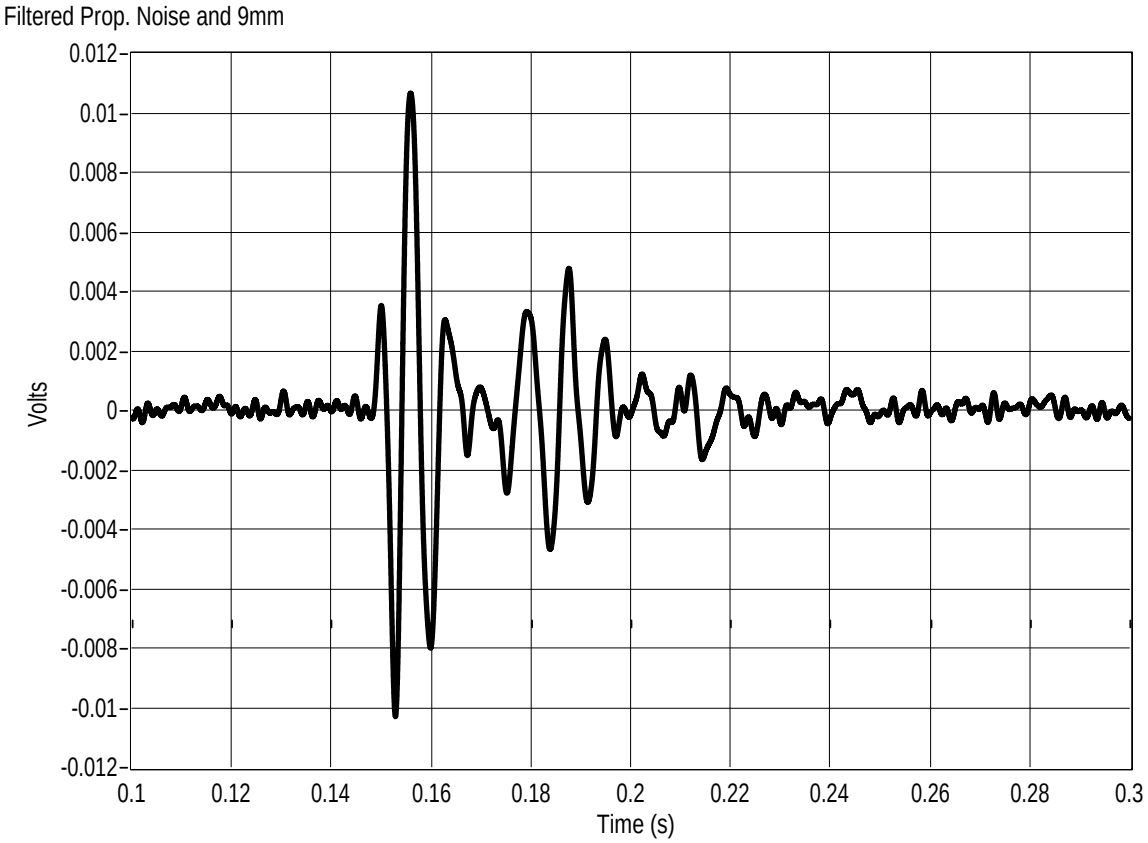

Figure 6.12: Filtered Propeller Noise with Gunshot

6.3 System Parameters

The measured system parameters are:

1. Weight

2. Power Consumption

3. Cost

The measurement of the sUAV weight includes the frame, motors, propellers, flight controller, ESCs, power distribution board, receiver, GPS, and required cabling. The various component weights can be seen in Table 6.1.

Table 6.1: Weight of System Components

Component	**Weight (g)**
sUAV	1520
Battery	416
Mic. Array	200
Interface PCB	45
ADS1278	36
myRIO	235
Housing	201
Module:	**717**
Total:	**2653**

Weight was a crucial metric being considered when developing this system. It was required that the weight of the module must fall within the payload capacity of the sUAV. Not only could a heavier module negatively affect flight time, but the distribution of weight could introduce moments of instability to the system. In order to account for this, a model was developed in Solidworks and rectified with measured date in order to monitor the weight distribution. The addition of the module on the top part of the sUAV shifted the center of gravity (CG) upwards about 1.6 in and sits closer to the position of the Pixhawk. The difference in CG can be seen when comparing Figure 6.13 and Figure 6.14.

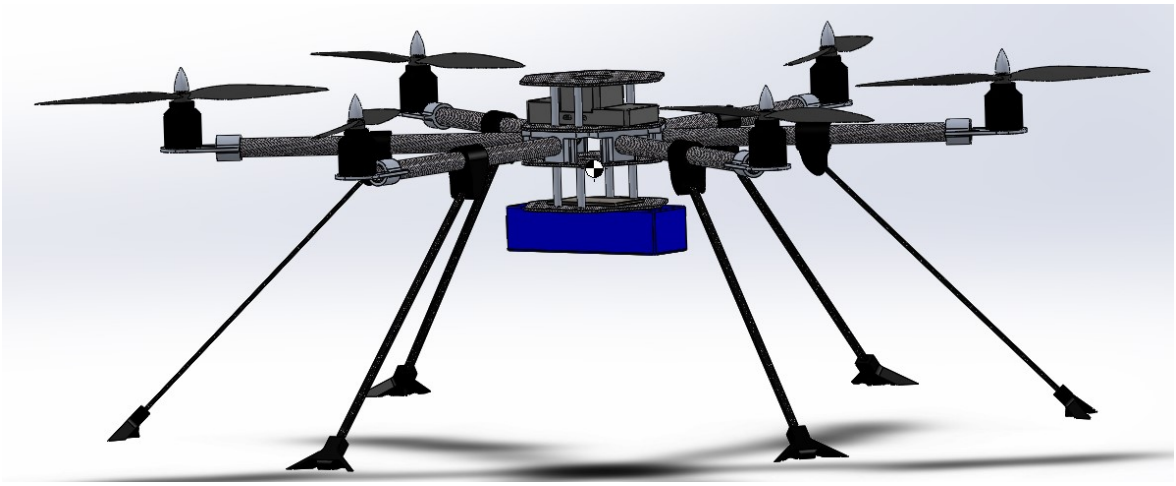

Figure 6.13: sUAS CG Model without Module

Figure 6.14: sUAS CG Model with Module aboard

The material cost of shop supplies like solder and heat shrink were not included in table 6.2. Shipping cost is not included.

Table 6.2: Cost of sUAV Components

Component	**Quantity**	**Cost (USD $)**
Frame	1	43.90
Battery	1	84.90
Motors	6	365.70
ESC	6	72.00
Power Distribution Board	1	7.75
Propellers	6	12.00
Pixhawk 2.1	1	238.00
GPS	1	58.00
Transmitter	1	110.00
Receiver	1	34.99
	Total:	**$1027.24**

The typical power consumption of the module at idle is categorized by components in Table 6.3. During operation, the characteristics of the ADC and the microphones remain relatively constant, but the power consumption of the myRIO can vary significantly with a maximum power consumption of 14W [39].

Table 6.3: Module Typical Electric Power Consumption

Component	**Voltage (V)**	**Current**	**Power**
ADS1278	1.8	4.5uA	8.1uW
	3.3	15.4mA	50.8mW
	5V	79.8mA	0.4W
		Total:	0.45W
Microphone	3.3	95.1uA	0.314mW
	(x8)	**Total:**	2.5mW
myRIO	9	0.3A	2.7
	Module Total:		3.2W

6.4 DOA Estimation

Initial test were developed to explore the accuracy of DOA estimation in real-time under various conditions. The initial evaluation of the impulse detection was completed by playing recorded gunshots indoors from a speaker at different distances from the array. The cross-correlation approach to detecting a distinct impulsive event works reliably under conditions where the SNR is high. The user-defined threshold for the detector could be adjusted in real time to account for varying SNR so that there were minimal false-positive detections. Given a correct detection of an impulsive noise, the module was able to successfully estimate DOA with an accuracy of approximately $\pm$ 7°. The DOA accuracy was evaluated by placing the speaker source at different locations with respect to the microphone array origin and comparing recording estimates against true values that were estimated using a tape measure.

CHAPTER 7: CONCLUSION

7.1 Summary of Results

The prototype system achieved the desired goals. It served as a proof of concept and successfully demonstrated that a lightweight, low-cost, source localization module can be successfully deployed onboard a sUAV while estimating both elevation and azimuth of an acoustic event. The application of the ADS1278 EVM-PDK joined with the myRIO embedded system provided a significant amount of computational power for reliably evaluating high rates of high-resolution data in real-time. The GCC-PHAT method works well for estimating TDOA of a sensor array made of closely packed microphones. The contribution of noise generated by the sUAV propellers can be substantially mitigated by the application of a digital low-pass filter with applications to gunshot-like impulses due to the fact that the majority of the frequency content falls outside the band of interest for those impulses. The acoustic localization application can be expanded to accomplish tasks beyond just large impulsive events like the ones explored in this thesis. The driver developed for the ADS1278 to function with the myRIO is a powerful tool that can be used to accomplish many DSP tasks beyond the scope of this work that require synchronous, high resolution sampling of multi channel analog data.

7.2 Future Work

There are many paths that this prototype system could follow in order to become a more accurate source localization device. A thorough evaluation of the system needs to be completed with the DOA estimates compared to accurate measurements of the true

DOA using laser range finders and laboratory quality measurement tools. The execution of the system needs to be evaluated with the sUAV in the air and with live gunshots at varying distances.

Measurements of the raw voltage from the microphones need to be represented in sound pressure level so that the effects of SNR can be better understood. An accurate algorithm could be employed that does not make the assumption of the acoustic wavefront propagating as a wave. This would include deriving a new solution to a set of nonlinear equations. The new algorithm would also develop an estimate for the range or distance to the acoustic source. This could be done by including the receiver signal strength into the search for a nonlinear solution.

A temperature sensor could be included into the system so that a more accurate estimate for the speed of sound could be made. There is also a plan to incorporate a camera with gimbal to point in the direction of the estimated DOA. The video could be relayed to a user in real-time so that a human could perform further evaluation. A PCB could be developed that is lighter and more compact that includes the necessary circuitry to perform the ADC and DSP on a single board. The PCB could then be used to develop a source localization module that can easily be deployed onto a commercially available sUAV.

Acoustic classification is another process that could be deployed onto the system. This would include distinguishing certain acoustic events from others. This could be used to prevent false-positive detections of acoustic events that are not of interest.

REFERENCES

[1] S. G Gupta, M. Ghonge, and P. Jawandhiya, "Review of unmanned aircraft system (uas)," vol. 9, 04 2013.

[2] R. P. Fernandes, J. A. Apolinário, and A. L. L. Ramos, "Bearings-only aerial shooter localization using a microphone array mounted on a drone," in *2017 IEEE 8th Latin American Symposium on Circuits Systems (LASCAS)*, pp. 1–4, Feb 2017.

[3] C. Reiff, T. Pham, M. F. Scanlon, and J. Noble, "Acoustic detection from aerial balloon platform," 2004.

[4] J. A. A. Rigel P. Fernandes, António L. L. Ramos, "Airborne doa estimation of gunshot acoustic signals using drones with application to sniper localization systems," 2017.

[5] R. P. Fernandes, A. Borzino, A. Ramos, and J. Apolinario, "Investigating the potential of UAV for gunshot DoA estimation and shooter localization," September 2016.

[6] FAA, "FAA aerospace forecast fy 2018-2038," 2017.

[7] FAA, "Small unmanned aircraft regulations (part 107)," July 2018.

[8] D. Reid, "A swarm of armed drones attacked a russian military base in syria," *CNBC*, January 2018.

[9] J. Wendle, "The fighting drones of ukraine," *Air and Space Magazine*, February 2018.

[10] A. Manikas, Y. I. Kamil, and M. Willerton, "Source localization using sparse large aperture arrays," *IEEE Transactions on Signal Processing*, vol. 60, pp. 6617–6629, Dec 2012.

[11] W. Van der Kloot, "Lawrence bragg's role in the development of sound-ranging in world war i," *Notes and Records*, vol. 59, no. 3, pp. 273–284, 2005.

[12] S. Griebel, *A Microphone Array System for Speech Source Localization, Denoising, and Dereverberation*. PhD thesis, Harvard University, April 2002.

[13] A. Ramos, *Acoustic Sniper Positioning Systems*. PhD dissertation, University of Oslo, January 2015.

[14] C. Knapp and G. Carter, "The generalized correlation method for estimation of time delay," *IEEE Transactions on Acoustics, Speech, and Signal Processing*, vol. 24, pp. 320–327, August 1976.

[15] W. E. Baker, *Explosions in Air*. University of Texas Press, 1973.

[16] R. C. Maher, "Acoustical characterization of gunshots," in *2007 IEEE Workshop on Signal Processing Applications for Public Security and Forensics*, pp. 1–5, April 2007.

[17] J. W. M. DuMond, E. R. Cohen, W. K. H. Panofsky, and E. Deeds, "A determination of the wave forms and laws of propagation and dissipation of ballistic shock waves," *The Journal of the Acoustical Society of America*, vol. 18, no. 1, pp. 97–118, 1946.

[18] R. C. Maher and S. R. Shaw, "Deciphering gunshot recordings," 2008.

[19] J. Bendat and A. Piersol, *Random Data*. Wiley, 1986.

[20] G. C. Carter, "Coherence and time delay estimation," *Proceedings of the IEEE*, vol. 75, pp. 236–255, Feb 1987.

[21] B. V. D. Broeck, A. Bertrand, P. Karsmakers, B. Vanrumste, H. V. hamme, and M. Moonen, "Time-domain generalized cross correlation phase transform sound source localization for small microphone arrays," in *2012 5th European DSP Education and Research Conference (EDERC)*, pp. 76–80, Sept 2012.

[22] I. L. Freire and J. A. Apolinário, "Doa of gunshot signals in a spatial microphone array: Performance of the interpolated generalized cross-correlation method," in *2011 Argentine School of Micro-Nanoelectronics, Technology and Applications*, pp. 1–6, Aug 2011.

[23] X. Cui, K. Yu, and S. Lu, "Direction finding for transient acoustic source based on biased tdoa measurement," *IEEE Transactions on Instrumentation and Measurement*, vol. 65, pp. 2442–2453, Nov 2016.

[24] HobbyKing, "Turnigy talon hexcopter (v1.0)." https://hobbyking.com/en_us/turnigy-talon-hexcopter-v1-0-carbon-fiber-frame-625mm.html?___store=en_us, 2018. Accessed: 2018-10-29.

[25] KDE Direct, *KDE2315XF-2050 Brushless Motor for Electric Multi-Rotor (sUAS) Series*, 2018.

[26] HobbyWing, "Arris simonk 30a 2-6s opto brushless esc." https://www.hobby-wing.com/arris-30a-opto-esc.html, 2018. Accessed: 2018-10-29.

[27] HeliPal, "Storm 14.8v 4000mah 30c pro series li-po battery (xt60)." http://www.helipal.com/storm-14-8v-4000mah-30c-pro-series-li-po-battery-xt60.html, 2018. Accessed: 2018-10-29.

[28] RayCorp, "Genuine gemfan 9045 (9x4.5) propellers by raycorp.." https://www.amazon.com/gp/product/B071ZQL16D/ref=oh_aui_search_detailpage?ie=UTF8&psc=1, 2018. Accessed: 2018-10-29.

[29] M. Systems, "Pdb power distribution board (matek systems)." https://www.amazon.com/dp/B071K945GL/ref=sspa_dk_detail_0?psc=1&pd_rd_i=B071K945GL&pf_rd_m=ATVPDKIKX0DER&pf_rd_p=f52e26da-1287-4616-824b-efc564ff75a4&pf_rd_r=4XY6S2F3ZD6JADAJ21CG&pd_rd_wg=zTBSY&pf_rd_s=desktop-dp-sims&pf_rd_t=40701&pd_rd_w=veX4o&pf_rd_i=desktop-dp-sims&pd_rd_r=82136e7d-d907-11e8-b1e4-5f3ea650bb69, 2018. Accessed: 2018-10-29.

[30] F. FPV, "Power module for pixhawk 2.1." https://www.foxtechfpv.com/power-module-for-pixhawk-2-1.html, 2018. Accessed: 2018-10-29.

[31] Dronecode, "Pixhawk 2.1 flight controller." https://docs.px4.io/en/flight_controller/pixhawk-2.html, 2018. Accessed: 2018-10-29.

[32] FrSKY, "Taranis qx7." https://www.frsky-rc.com/product/taranis-q-x7-2/, 2018. Accessed: 2018-10-29.

[33] FrSKY, "X8r." https://www.frsky-rc.com/product/x8r/, 2018. Accessed: 2018-10-29.

[34] R. Shop, "Here gnss for pixhawk 2.1." https://www.robotshop.com/en/here-gnss-pixhawk-21.html, 2018. Accessed: 2018-10-29.

[35] Adafruit, "Adafruit silicon mems microphone breakout - spw2430." https://www.adafruit.com/product/2716, 2018. Accessed: 2018-10-29.

[36] Knowles, *SPW2430HR5H-B Datasheet*, February 2014. Rev. A.

[37] Texas Instruments, *Quad/Octal, Simultaneous Sampling, 24-Bit Analog-to-Digital Converters datasheet*, April 2007. Rev. F.

[38] Texas Instruments, *ADS1x7xEVM User's Guide*, February 2012. Rev. A.

[39] National Instruments, *myRIO 1900 User Guide and Specifications*, May 2016.

[40] Texas Instruments, *Designing Modular EVMs for Data Acquisition Products*, November 2003. Rev. A.

[41] Texas Instruments, *250mA Ultra-Low-Noise Low-Iq Low-Dropout Regulator Datasheet*, April 2012. Rev.N.

[42] R. C. Maher, "Modeling and signal processing of acoustic gunshot recordings," in *2006 IEEE 12th Digital Signal Processing Workshop 4th IEEE Signal Processing Education Workshop*, pp. 257–261, Sept 2006.

APPENDIX A: NOMENCLATURE

ADC	Analog to digital Converter
CPU	Central Processing Unit
c	Speed of Sound in Air
COTS	Commercial off-the-Shelf
DAQ	Data Acquisition
dB	Decibels
DMA	Direct Memory Access
DOA	Direction of Arrival
DSP	Digital Signal Processing
ESC	Electronic Speed Controller
ESPRIT	Estimation of Signal Parameters via Rotational Invariance Techniques
EVM-PDK	Evaluation Module-Product Development Kit
FAA	Federal Aviation Administration
FFT	Fast Fourier Transform
FIFO	First-in First-out
FPGA	Field Programmable Gate Array
GCC-PHAT	Generalized Cross Correlation with Phase Transform
LLS	Linear Least Squares
LOS	Line of Sight
MEMS	Micro Electro-Mechanical System
MUSIC	Multiple Signal Classification

NI	National Instruments
NLS	Non-Linear Least Squares
PCB	Printed Circuit Board
PSD	Power Spectral Density
Rxy	Cross Correlation Function
SNR	Signal-to-Noise Ratio
SPI	Serial Peripheral Interface
SPL	Sound Pressure Level
sUAS	Small Unmanned Aircraft System
sUAV	Small Unmanned Aircraft Vehicle
TDOA	Time Difference of Arrival
TI	Texas Instruments
VI	Virtual Instrument
VTOL	Vertical Take-off and Landing
θ	Elevation
ϕ	Azimuth
$\tau_{i,j}$	Time Delay Between Channels i and j

APPENDIX B: HARDWARE AND SOFTWARE DIAGRAMS

Figure B.1: Full Assembly of System

Table B.1: Position of Microphones Relative to Origin

Microphone	**Position (cm)**		
Number	**X**	**Y**	**Z**
1	0.0	0.0	28.3
2	0.0	20.0	20.0
3	-17.3	-10.0	20.0
4	17.3	-10.0	20.0
5	-14.2	-14.2	-20.0
6	14.2	-14.2	-20.0
7	-14.2	14.2	-20.0
8	14.2	14.2	-20.0

Table B.2: Cost of Module Components

Component	**Quantity**	**Cost (USD $)**
Microphones	8	39.60
Carbon Fiber Rods	2	33.98
myRIO MXP Cable	1	5.99
24 Pin Cable	1	2.99
myRIO	1	548.00
ADS1278 EVM-PDK	6	149.00
Interface Board	1	29.70
	Total:	**$809.26**

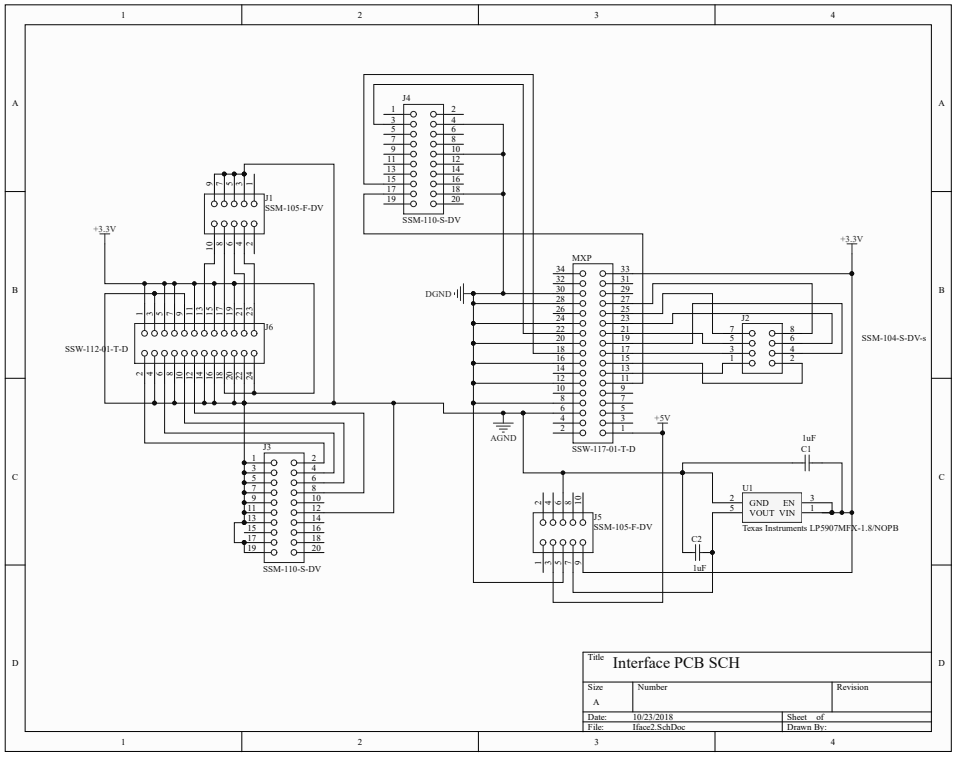

Figure B.2: Interface PCB Schematic

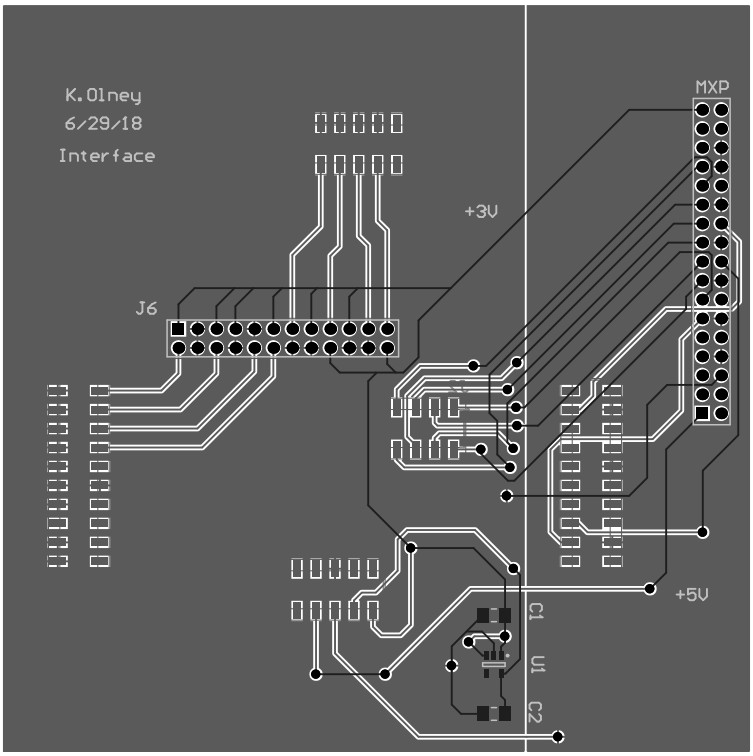

Figure B.3: Interface PCB Layout

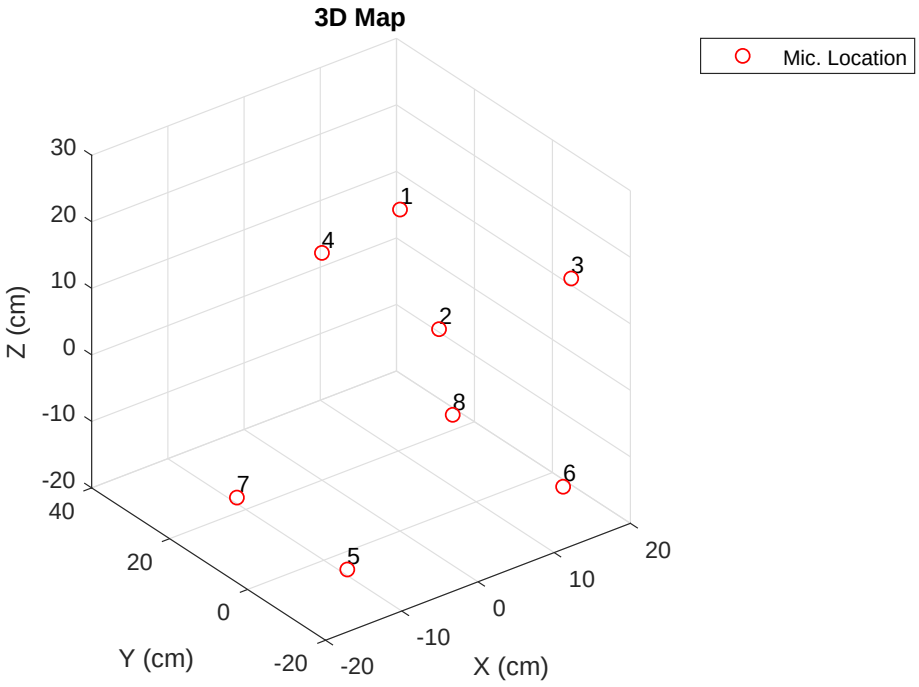

Figure B.4: 3D Model of Mic Positions

APPENDIX C: RECORDED CALIBERS

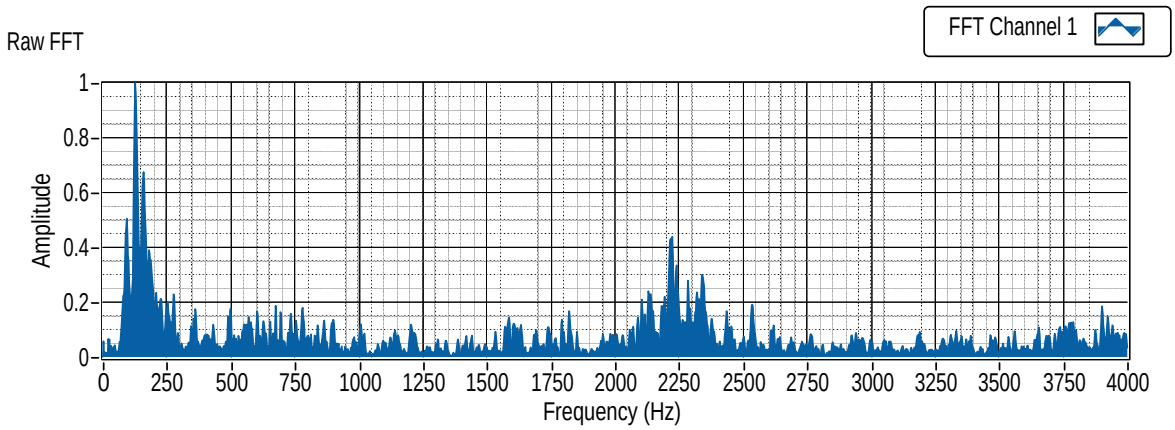

Figure C.1: Extended Band FFT of 9mm Gunshot